DRIVING TURBULENCE AND TRIGGERING STAR FORMATION BY IONIZING RADIATION

MATTHIAS GRITSCHNEDER[1], THORSTEN NAAB[1], STEFANIE WALCH[1], ANDREAS BURKERT[1], AND FABIAN HEITSCH[2]
[1] Universitäts-Sternwarte München, Scheinerstr. 1, D-81679 München, Germany; gritschm@usm.uni-muenchen.de
[2] Department of Astronomy, University of Michigan, Ann Arbor, MI 48109-1042, USA

ABSTRACT

We present high-resolution simulations on the impact of ionizing radiation of massive O stars on the surrounding turbulent interstellar medium (ISM). The simulations are performed with the newly developed software iVINE which combines ionization with smoothed particle hydrodynamics (SPH) and gravitational forces. We show that radiation from hot stars penetrates the ISM, efficiently heats cold low-density gas and amplifies overdensities seeded by the initial turbulence. The formation of observed pillar-like structures in star-forming regions (e.g. in M16) can be explained by this scenario. At the tip of the pillars gravitational collapse can be induced, eventually leading to the formation of low-mass stars. Detailed analysis of the evolution of the turbulence spectra shows that UV radiation of O stars indeed provides an excellent mechanism to sustain and even drive turbulence in the parental molecular cloud.

Key words: ISM: structure – methods: numerical – stars: formation – turbulence – ultraviolet: ISM

1. INTRODUCTION

Some of the most spectacular structures in the molecular interstellar medium (ISM) are observed in the vicinity of hot O/B stars or associations, e.g., the Horsehead nebula (B33), the three pillars of creation in M16, and the Elephant trunk (BRC37) in IC1396. For the pillars in M16, Sugitani et al. (2002) find a head-to-tail structure with the denser head pointing toward the OB stars of NGC661. In addition, young stellar objects (YSOs) are present at the tips of the pillars. In the Horsehead nebula Ward-Thompson et al. (2006) report two core-like structures that might undergo subsequent gravitational collapse. Very recent observations by Ikeda et al. (2008) report several YSOs close to the tip of BRC37. As a common feature, these pillar-shaped nebulae point toward a source of ionizing radiation and show signs of present or future star formation at their tips.

Up to now, the precise physical processes leading to the formation of these structures are not fully understood. The morphologies suggest that feedback effects of UV radiation and winds of massive stars play an important role in the formation of the pillars. In addition, the radiation might have a strong impact on the overall evolution of the parental cloud. Furthermore, molecular clouds are observed to be highly turbulent structures. There is evidence that this turbulence can support the clouds against gravitational collapse and thereby control star formation. As hydrodynamic and magnetohydrodynamic (MHD) turbulence decays rather quickly, the only way to explain this high level of turbulence would be to drive the turbulence—either on large scales by, i.e., supernova explosions or on small scales from within the cloud by stellar outflows, winds or ionization (see, e.g., Elmegreen & Scalo 2004; Mac Low & Klessen 2004, for reviews). The possibility of ionization-driven turbulence has been indicated by, e.g., semi-analytic models of Krumholz et al. (2006). In this Letter, we test the hypothesis using high-resolution numerical simulations with the newly developed code iVINE (Gritschneder et al. 2009, hereafter G09).

On the theoretical side progress has been made since Elmegreen et al. (1995) first presented two-dimensional, grid-based simulations showing that the expansion of an H II region into the surrounding ISM can trigger star formation by sweeping up the cold material. This is called "collect and collapse." Another proposed scenario is the "radiation-driven implosion,"

where pre-existing density structures are driven into collapse (see, e.g., Bertoldi 1989; Kessel-Deynet & Burkert 2003; G09).

For the numerical treatment of radiation in simulations several codes have been developed (see Iliev et al. 2006 and references therein). Recent applications for the treatment of ionizing radiation in grid-based codes include, e.g., Mellema et al. (2006) and Krumholz et al. (2007). In SPH codes implementations have been presented by Dale et al. (2005), Pawlik & Schaye (2008), and Altay et al. (2008). Simulations by Dale et al. (2007) show that ionizing radiation can slightly enhance the formation of cores in a globally unbound molecular cloud of $10^4 \, M_\odot$. With their choice of initial conditions, the positive feedback, the additional or faster formation of cores, outweighs the negative feedback, the disruption of cores. All these applications calculate the effect of a point source on the surrounding medium, thereby focusing much more on the global effect of the ionization. However, neither the detailed morphology of the gas nor the impact of the ionizing radiation on the turbulence has been investigated so far.

2. INITIAL CONDITIONS

We set up a box of gas with sides 4 pc long at a temperature of $T_{\rm cold} = 10$ K and a mean number density of $\bar{n} = 300$ cm^{-3}, which resembles a slightly denser part of a molecular cloud. The gas mass in the box is $474 \, M_\odot$ which corresponds to 25 Jeans masses. To mimic initial turbulence we employ a supersonic turbulent velocity field (Mach 10) with a steep power law $E(k) \propto k^{-2}$, where only the largest modes $k = 1, \ldots, 4$ are populated initially. This setup is allowed to freely decay under the influence of isothermal hydrodynamics simulated with the tree/SPH code VINE (Wetzstein et al. 2008; Nelson et al. 2008). The individual particle time steps in VINE are determined by using an accuracy parameter of $\tau_{\rm acc} = 1.0$ and a Courant–Friedrichs–Lewy (CFL) tolerance parameter of $\tau_{\rm CFL} = 0.3$. We also use an additional time-step criterion based on the maximum allowed change of the smoothing length with an accuracy parameter of $\tau_{\rm h} = 0.15$.

After ≈ 1 Myr, a Kolmogorov-like power law with $E(k) \propto k^{-\frac{5}{3}}$ is well established on all resolvable scales. The velocities now correspond to Mach 5. This initial setup with the turbulent
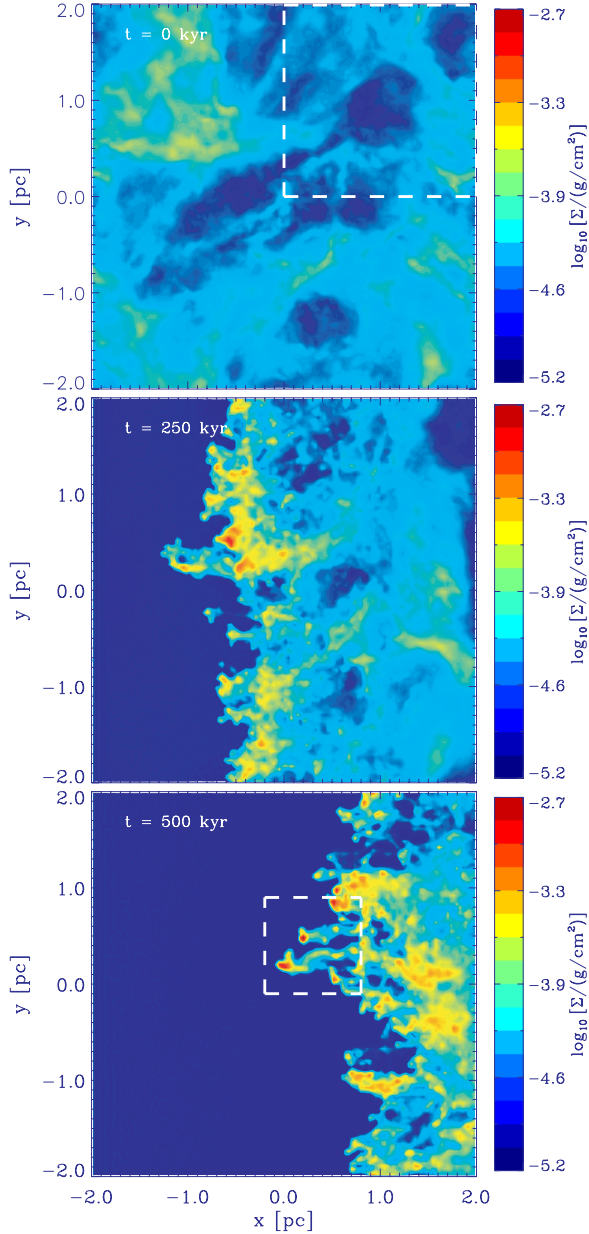
Figure 1. Evolution of the turbulent ISM under the influence of UV radiation impinging from the left-hand side. Color coded is the surface density projected along the z-direction. The time of the snapshot is increasing from top to bottom.
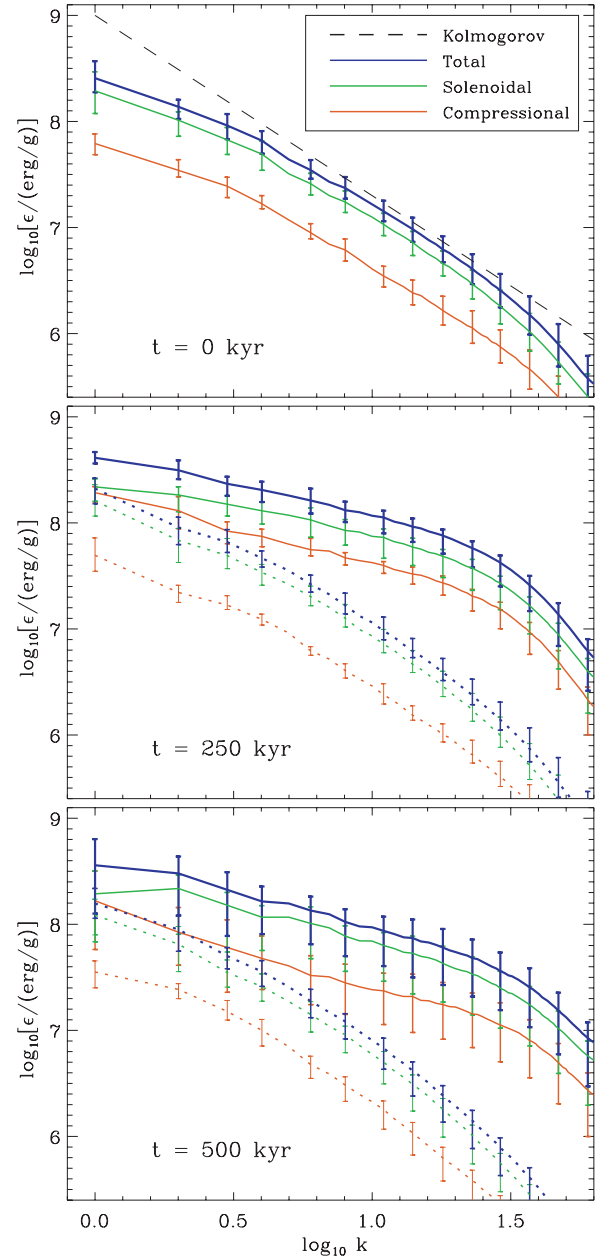

Figure 2. Evolution of the density-weighted power spectra: plotted is the logarithm of the wavenumber vs. the logarithm of the specific kinetic energy. Solid lines denote the run with ionization, dotted lines the control run without ionization. Plotted is the mean value of the spectra in the four different backward cubes; the error bars show the minimum and maximum values. Blue: total specific kinetic energy; green: solenoidal modes; red: compressional modes; dashed: Kolmogorov power law.

velocities is shown in Figure 1 (top panel); the corresponding power spectrum is shown in Figure 2 (top panel).

With these turbulent initial conditions we perform two simulations, one with and one without the inclusion of ionization. To account for the UV radiation of a young massive star, we use iVINE (G09), a new parallel implementation of ionizing radiation in the tree/SPH code VINE. Here we assume plane–parallel infall of UV radiation onto one transparent side of the simulated area, which enables us to perform simulations at yet unmatched high resolution. From the surface, the radiation is propagated by a ray-shooting algorithm. The size of the rays is determined by the smoothing length of the SPH particles, i.e., the width a particle occupies. Along these rays the radiation is calculated. This provides us with an ionization degree η for each SPH particle, which is then used to assign a new temperature to

each particle by linear interpolation:

$$T = T_{\rm hot} \cdot \eta + T_{\rm cold} \cdot (1 - \eta), \qquad (1)$$

where $T_{\rm cold} = 10$ K is the initial temperature of the cold, unionized gas and $T_{\rm hot} = 10^4$ K is the average temperature of the ionized gas (see, e.g., Shu 1991). The gas is assumed to be atomic hydrogen. Both gas components are close to thermal equilibrium, since the heating and cooling timescales are much shorter than the dynamical timescales. We treat the gas with an isothermal equation of state ($\gamma = 1$) as, for the density range in our simulations, heating and cooling should balance each other to approximate isothermality (see, e.g., Scalo et al.

1998). However, in reality the situation is more complicated. Recent simulations by Glover & Mac Low (2007) indicate an equation of state of the thermal equilibrium gas which is softer than isothermal ($\gamma = 0.7$–0.8). For a detailed prescription of the iVINE code along with several analytical test cases see G09. In the simulations presented here the radiation was calculated on more than $(60)^2$ rays, with the additional inclusion of five levels of refinement, leading to a spatial resolution of 2×10^{-3} pc in the radiation. The photon flux per unit time and area is set to $F_{\mathrm{Ly}} = 5 \times 10^9$ photons cm^{-2} s^{-1}, allowing the radiation to penetrate the first 10% of the cloud immediately. This corresponds to setting up our simulation to be right at the border of the Strömgren sphere (Strömgren 1939), which can be immediately ionized by an O star or association.

The radiation is impinging from the negative x-direction. Hydrodynamics is calculated with periodic boundaries in the y- and z-directions. The boundary is assumed to be reflecting in the negative x-direction to represent conservation of flux toward the star, whereas in the positive x-direction, the gas is allowed to stream away freely. Gravitational forces are calculated without boundaries. This is valid as the free-fall time of the whole simulated area is $t_{\mathrm{ff}} \approx 3$ Myr, which is much larger than the simulation time. To ensure a correct integration of all quantities, we use the individual time-stepping scheme of VINE with the same parameters as for the freely decaying turbulence (see above). For the tree-based calculation of gravitational forces, we use a multipole acceptance criterion (MAC; Springel et al. 2001) with a tree accuracy parameter of $\theta = 5 \times 10^{-4}$. The correct treatment of the ionization and the resulting acceleration of the particles are obtained by a modified CFL condition as discussed in G09. The simulations are performed with 2×10^6 gas particles on an SGI Altix 3700 Bx2 supercomputer. The entire calculation took approximately 100 wall clock hours on 16 CPUs.

3. RESULTS

3.1. Morphology and Formation of Cores

At the beginning of the simulation the R-type front immediately reaches into the first 10% of the box, with the radiation penetrating further into the low-density parts of the cold gas. After a hydrodynamical crossing timescale of the hot gas ($t_{\mathrm{hot}} \approx 30$ kyr)[3] the ionized gas reacts to its increase in temperature and starts to exert pressure on the cold gas. The cold gas is compressed and pushed away from the source, leading to a systematic velocity in the x-direction. At the same time the radiation has penetrated and ionized the ISM along channels of low-density gas. Now these low-density regions expand and start compressing the denser, un-ionized regions especially tangential to the direction of radiation. Thus, the pre-existing density structures, which are seeded by the turbulent initial conditions, get enhanced as shown in Figure 1.

The combination of overall and tangential compression leads to elongated structures that keep sweeping up cold gas. After ≈ 250 kyr (Figure 1, middle panel) the dominant structures are already excavated by the combination of radiation and the pressure of the hot gas. From now on the evolution is mainly dominated by the hydrodynamic interactions between the hot and cold phases of the gas.

After ≈ 500 kyr (Figure 1, bottom panel) the morphology is remarkably reminiscent of the observed structures. The pillars

in our simulations are indeed very complex structures with a corkscrew type, torqued morphology and show rotational motion around their main axis, as is observed (Gahm et al. 2006). Up to now it has been suggested that these complex morphologies arise due to magnetic fields, which are not included in our simulations. It is very likely that the pillars in M16 are a snapshot of the formation scenario proposed here. At this stage the densest region (indicated by the center of the white box in Figure 1, bottom panel) undergoes gravitational collapse, the simulation is slowed down considerably, and we terminate it. Future simulations with the inclusion of, e.g., sink particles to avoid the detailed calculation of the further gravitational collapse leading to low-mass stars will allow us to trace the subsequent evolution of the whole region. We call the most prominent feature in the white box in Figure 1 (bottom panel) "pillar I" and the second largest "pillar II"; the collapsing compact core is at the tip of pillar II. Their respective masses are $M_{\mathrm{pillarI}} = 12.3\,M_\odot$, $M_{\mathrm{pillarII}} = 8.1\,M_\odot$, and $M_{\mathrm{core}} = 0.7\,M_\odot$. The compact core is defined as all material with a number density above $n_{\mathrm{crit}} = 10^7$ cm^{-3} in a region of $R_{\mathrm{crit}} = 0.02$ pc around the peak density (see G09). Observations show that star formation is taking place close to the tips of the evolving structures (Snider et al. 2007). The same is true for our simulations. In the process of sweeping up, the dense material lags behind, gaining less momentum, and thus leading to very high-density enhancements near the radiation front. In contrast, the simulation without UV radiation does not show any signs of gravitational collapse.

Overall the scenario is very similar to the "collect and collapse" model, as the denser regions would not collapse on their own on the timescale simulated and the sweeping up of material plays a vital role. We call it "collect and collapse with turbulent seeds."

3.2. Turbulent Evolution

For the discussion of the evolution of the density-weighted spectra from the run with ionization, we perform a control run with the same initial conditions and accuracy parameters as the main simulation but without the inclusion of UV radiation. In the comparison run, no sign of star formation can be detected. This is reasonable, since the cloud is not set up to become gravitationally unstable as the total time of the simulation is much less than t_{ff}. The comparison is shown at $t = 0$ kyr, $t = 250$ kyr, and $t = 500$ kyr (Figure 2). We analyze the turbulent spectrum in four cubic domains in the backward domain of the simulation, spanning 2 pc in each direction (one is indicated in Figure 1, top panel; the other three are shifted in the negative y- and z-directions, respectively). Thus, it is guaranteed that there is always enough cold gas in the volume to achieve sensible results. To avoid a bias by either the ionized gas or the forming high-density regions, we take into account only gas with a number density 10^2 cm$^{-3} < n < 10^4$ cm^{-3}. The particles are binned on a $(128)^3$ cubic grid by using a kernel-weighted binning routine (as, e.g., in Kitsionas et al. 2008). Based on this grid, we calculate the density-weighted spectra by substituting $\mathbf{v}$ with $(\rho/\bar\rho)^{1/2}(\mathbf{v} - \mathbf{v}_{\mathrm{RMS}})$ before the Fourier transformation. $\mathbf{v}_{\mathrm{RMS}}$ is the average velocity in each of the three components. The specific turbulent kinetic energy in the Fourier space is then given as

$$\epsilon_{\mathrm{kin,turb}} = \tfrac{1}{2}(\mathbf{v}' \cdot \bar{\mathbf{v}}'), \qquad (2)$$

where $\mathbf{v}'$ and $\bar{\mathbf{v}}'$ are the Fourier transform of the substituted velocity and its complex conjugate, respectively. By mapping

---

[3] This timescale is calculated by taking the sound speed of the hot ionized gas $c_{\mathrm{s,hot}} = 13.1$ pc/Myr and the average penetration length of the ionization of 0.4 pc into account.

the $\epsilon_{\rm kin,turb}$ cube to wavenumbers $\mathbf{k}$, the specific energy in the compressional, curl-free modes can be calculated as

$$\epsilon_{\rm com} = \epsilon_{\rm turb,kin} \frac{(\mathbf{v'} \cdot \mathbf{k})(\mathbf{\bar{v}'} \cdot \mathbf{k})}{(\mathbf{k} \cdot \mathbf{k})(\mathbf{v'} \cdot \mathbf{\bar{v}'})}. \qquad (3)$$

The specific energy in the solenoidal or incompressible, divergence-free modes is then given by $\epsilon_{\rm sol} = \epsilon_{\rm kin,turb} - \epsilon_{\rm com}$. We construct the spectra by collecting the energy in the different wavenumber intervals (see Kitsionas et al. 2008, for details). The total spectra as well as the solenoidal and compressional parts are shown in Figure 2.

The initial spectrum at $t = 0$ kyr (Figure 2, top panel) resembles quite well a power law, even though the large-scale (low-k) modes are lower, as the initial conditions are not produced by driven but by freely decaying turbulence. The slope is similar to a Kolmogorov law. Approximately 25% of the total turbulent energy is contained in the compressional modes.

At $t = 250$ kyr (Figure 2, middle panel), there is already a distinct difference between the two spectra. The control run keeps the power-law shape and dissipates energy. In the ionization case, the power is strongly increased on all scales. The increase is pronounced for $k > 10$, corresponding to scales < 0.2 pc. An interesting feature is the rise in the compressional modes, where now 39% of the total turbulent energy is contained, whereas in the comparison run this ratio stays at 25%. This clearly shows that the energy of the radiation is transferred into compression of the cold gas via the hot gas. The increase is in the turbulent energy itself and not correlated with the overall bulk motion in the x-direction, since the mean velocity is subtracted separately in each direction before the Fourier transform.

After $t = 500$ kyr (Figure 2, bottom panel), these differences are even more pronounced. The kinetic energy in the cold gas is now a factor of 4 higher than in the run without ionization. Approximately 33% of the total turbulent energy is now contained in the compressional modes. This suggests that after an initial phase of high compression the system starts to relax.

Including the mass in the respective region and density range the total turbulent energy can be calculated. The initial turbulent energy is $E_{\rm turb} = 2.1 \times 10^{45}$ erg, the final turbulent energy (at $t = 500$ kyr) is $E_{\rm ion} = 4.3 \times 10^{45}$ erg, and $E_{\rm nion} = 1.1 \times 10^{45}$ erg in the ionized and un-ionized case, respectively. Thus, the input of turbulent energy per unit volume and unit time averaged over the simulation time when comparing the run with ionization to the case of freely decaying turbulence is $\dot{e}_{\rm turb} = 2.1 \times 10^{-25}$ erg s^{-1} cm^{-3}. By using the simplified assumption that the UV radiation is absorbed isotropically in the entire simulation volume, the amount of energy contained in the ionizing radiation for the chosen flux $F_{\rm Ly}$ is $\dot{e}_{\rm Ly} = 3.5 \times 10^{-20}$ erg s^{-1} cm^{-3}. Compared to the estimates of Matzner (2002) and Mac Low & Klessen (2004), our radiative energy is several orders of magnitude higher, since we look at the direct surrounding of an O star instead of averaging over an entire galaxy. Nevertheless, the conversion efficiency of ionization into turbulent motion of the cold gas is in our case $\sigma = \dot{e}_{\rm turb}/\dot{e}_{\rm Ly} \approx 2 \times 10^{-5}$, which is an order of magnitude higher than their estimate of $\sigma \approx 2 \times 10^{-6}$ for the Milky Way. Our highly resolved simulations show that ionizing radiation from an O star or association provides a much more efficient mechanism to drive and sustain turbulence in the parental molecular cloud than was previously estimated. However, this is still the energy input into the local environment in contrast to the average input rate on galactic scales derived by Mac Low & Klessen (2004). On the larger scales, it does not appear to contribute as significantly as, e.g., supernova explosions.

4. DISCUSSION

We have shown in this Letter that the observed pillar-like structures around O stars as well as the gravitational collapse at the tip of the pillars can result from the impact of the ionizing radiation of massive O stars on a turbulent molecular cloud. In addition, the turbulent energy in the cold gas is increased by a factor of 4, especially in the compressional modes. Both effects are due to the same mechanism: the ionization can heat the gas along channels of low density, thereby compressing gas at higher density into filaments. Close to the source of ionization, this leads to the excavation of pillar-like structures with triggered gravitational collapse at their tips. Further away from the source front, the structures have not yet fully developed; nevertheless the effect of compression is clearly visible in the turbulent energy spectra.

Even though we find striking similarities between our simulations and observations, one has to bear in mind that this is a simplified approach which does not involve full radiative transfer. Ionized gas which gets shaded is assumed to cool immediately without affecting the adjacent structures. In addition, the shaded gas does not get ionized and heated by the recombination radiation of the ionized gas surrounding it. This might influence the precise shape of the structure behind the tip. Moreover, the thin surface layers around each pillar where cold and hot gas are mixing cannot be resolved, although they might be crucial for the precise understanding of the temperature and the chemical composition of these structures. Nevertheless, our simulations indicate that these detailed effects are of minor importance to explain the global picture, i.e., the overall structure and mass assembly of the pillars observed. Stellar winds might have an additional impact. Although O stars have very powerful winds which can reach velocities of up to 1000 km s^{-1}, our models suggest that ionizing radiation alone can reproduce most observed features.

The straightforward combination of hydrodynamics and ionizing radiation together with a standard turbulent model and typical parameters for molecular clouds leads to morphologies consistent with observed objects like pillars and collapsing cores. The similarities suggest that ionizing radiation plays a major role not only in shaping the parental cloud, but also in triggering secondary star formation. Furthermore, the overall turbulent kinetic energy in the cold gas is increased significantly.

REFERENCES

Altay, G., Croft, R. A. C., & Pelupessy, I. 2008, MNRAS, 386, 1931
Bertoldi, F. 1989, ApJ, 346, 735
Dale, J. E., Bonnell, I. A., Clarke, C. J., & Bate, M. R. 2005, MNRAS, 358, 291
Dale, J. E., Clark, P. C., & Bonnell, I. A. 2007, MNRAS, 377, 535
Elmegreen, B. G., Kimura, T., & Tosa, M. 1995, ApJ, 451, 675
Elmegreen, B. G., & Scalo, J. 2004, ARA&A, 42, 211
Gahm, G. F., Carlqvist, P., Johansson, L. E. B., & Nikolić, S. 2006, A&A, 454, 201
Glover, S. C. O., & Mac Low, M.-M. 2007, ApJS, 169, 239

Gritschneder, M., Naab, T., Burkert, A., Walch, S., Heitsch, F., & Wetzstein, M. 2009, MNRAS, 393, 21

Ikeda, H., et al. 2008, AJ, 135, 2323

Iliev, I. T., et al. 2006, MNRAS, 371, 1057

Kessel-Deynet, O., & Burkert, A. 2003, MNRAS, 338, 545

Kitsionas, S., et al. 2008, arXiv:0810.4599

Krumholz, M. R., Matzner, C. D., & McKee, C. F. 2006, ApJ, 653, 361

Krumholz, M. R., Stone, J. M., & Gardiner, T. A. 2007, ApJ, 671, 518

Mac Low, M.-M., & Klessen, R. S. 2004, Rev. Mod. Phys., 76, 125

Matzner, C. D. 2002, ApJ, 566, 302

Mellema, G., Arthur, S. J., Henney, W. J., Iliev, I. T., & Shapiro, P. R. 2006, ApJ, 647, 397

Nelson, A. F., Wetzstein, M., & Naab, T. 2008, arXiv:0802.4253

Pawlik, A. H., & Schaye, J. 2008, MNRAS, 389, 651

Scalo, J., Vazquez-Semadeni, E., Chappell, D., & Passot, T. 1998, ApJ, 504, 835

Shu, F. H. 1991, The Physics of Astrophysics II: Gas Dynamics (New York: University Science Books), 429

Snider, K. D., Hester, J. J., Desch, S. J., Healy, K. R., & Bally, J. 2007, arXiv:0711.1515

Springel, V., Yoshida, N., & White, S. D. M. 2001, New Astron., 6, 79

Strömgren, B. 1939, ApJ, 89, 526

Sugitani, K., et al. 2002, ApJ, 565, L25

Ward-Thompson, D., Nutter, D., Bontemps, S., Whitworth, A., & Attwood, R. 2006, MNRAS, 369, 1201

Wetzstein, M., Nelson, A. F., Naab, T., & Burkert, A. 2008, arXiv:0802.4245